A numerical study of flow crossover between adjacent flow channels in a proton exchange membrane fuel cell with serpentine flow field

Zhongying Shi, Xia Wang*

Department of Mechanical Engineering, Oakland University, Rochester, MI 48309, United States

ABSTRACT

The focus of this paper is to study the flow crossover between two adjacent flow channels in a proton exchange membrane (PEM) fuel cell with serpentine flow field design in bipolar plates. The effect of gas diffusion layer (GDL) deformation on the flow crossover due to the compression in a fuel cell assembly process is particularly investigated. A three-dimensional structural mechanics model is created to study the GDL deformation under the assembly compression. A three-dimensional PEM fuel cell numerical model is developed in the aforementioned deformed domain to study the flow crossover between the adjacent channels in the presence of the GDL intrusion. The models are solved in COMSOL Multiphysics—a finite element-based commercial software package. The pressure, velocity, oxygen mass fraction and local current density distribution are presented. A parametric study is conducted to quantitatively investigate the effect of the GDL's transport related parameters such as porosity and permeability on the flow crossover between the adjacent flow channels. The polarization curves are also examined with and without the assembly compression considered. It is found that the compression effect is evident in the high current density region. Without considering the assembly compression, the fuel cell model tends to over-predict the fuel cell's performance. The proposed method to simulate the crossover with the deformed computational domain is more accurate in predicting the overall performance.

© 2008 Elsevier B.V. All rights reserved.

1. Introduction

The bipolar plate is an important component of proton exchange membrane (PEM) fuel cells. The flow field design in the bipolar plate influences the heat, mass and current transport inside fuel cells in a complex manner. Li [1] recognized an appropriate configuration of the flow field design in the bipolar plate as the most important strategy to handle water management issues. The basic flow field designs in the bipolar plate include: serpentine channel arrangement, parallel channel arrangement (also called conventional or straight arrangement) and interdigitated channel arrangement, as shown in Fig. 1. The serpentine design is one of the most widely used flow channel configurations, especially in small fuel cells [2].

The serpentine channel design has several parallel channels connected in series by U turns. The problems of gas bubble or liquid droplet blockage in a parallel channel design are less serious in the serpentine design since any block in a single serpentine channel will build a high-pressure region which moves the liquid or bubble and thus resolves the blockage. The total length of a single serpentine channel is several meters depending on the active area of fuel cells, while the cross sectional dimension is usually 0.5–1 mm. For example, for a 100 cm^2 fuel cell, if the width of the channel and bipolar plate shoulder is 1 mm, the total length of the flow channel is around 5 m. This large difference in dimensions creates a pressure difference between two adjacent flow channels which is high enough to introduce the flow crossover from one flow channel to the other through the porous gas diffusion layer (GDL). Some researchers define this effect as the "channel to channel crossover" [3]. In this study, the flow crossover between channels will be used to describe this phenomenon.

The flow crossover between channels enhances the mass transport of the reactant to the reaction site at the catalyst layer, which thus improves the overall performance of fuel cells. Park and Li [2] predicted that 40% of the inlet flow does not follow the channel in the bipolar plate, but instead crosses the land area between two adjacent channels through the GDL. Dutta et al. [4] found that the flow crossover between channels leads to an unexpected pressure drop compared to the flow in the straight channel. Sun and co-workers [3,5,6] developed a pure hydraulic model to show that the flow crossover also has a significant influence on the pressure variation through the channel, and tends to decrease the pressure drop. A similar phenomenon was found to be important in a direct methanol fuel cell [7]. Pharoah [8] found that the in-plane permeability of the GDL is the parameter of importance in affecting the

---

* Corresponding author. Tel.: +1 248 370 2224.
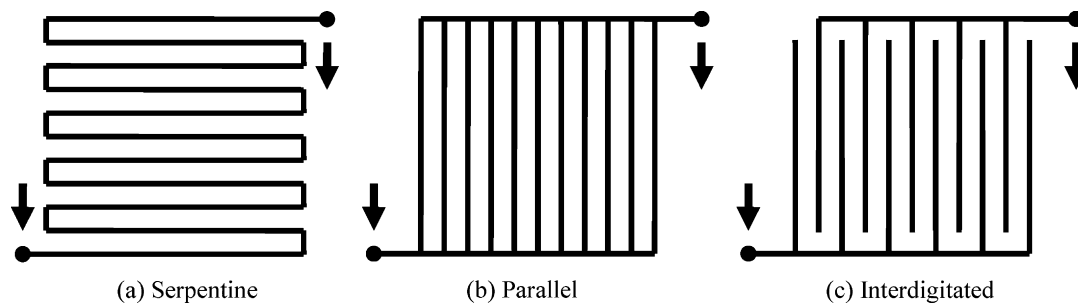*E-mail address:* wang@oakland.edu (X. Wang).

Fig. 1. Basic flow field configuration of the single PEM fuel cell channel. (a) Serpentine; (b) parallel; (c) interdigitated.

flow crossover between channels in a serpentine flow channel. In summary, the flow crossover between adjacent channels in a single serpentine flow channel design is crucial in the PEM fuel cell operation, and it should not be ignored in the fuel cell design and numerical simulation.

Permeability and porosity of the GDL are two of the key parameters that determine the flow crossover effect. These two parameters vary during the fuel cell assembly process. The porosity of the GDL will decrease especially under the shoulder of the bipolar plate due to the assembly compression [9–15], which will affect the permeability and then flow transport through the GDL. Lai et al. [16] recently investigated the effect of gas diffusion media intrusion on the performance of a PEM fuel cell. It was found that a 5% variation in gas diffusion media intrusion can result in a 20% reduction of reactant flow in the most intruded channel. The objective of this paper is to investigate the effects of flow crossover on the performance of a fuel cell with a serpentine flow channel design with the assembly compression effects considered. Firstly, a numerical model will be developed to simulate the porous GDL's deformation under assembly compression. A three-dimensional PEM fuel cell model will then be developed based on the deformed domain from the GDL's deformation model. The effects of flow crossover between adjacent channels on the fuel cell performance will be studied. The three-dimensional fuel cell model being developed includes the momentum transport, mass transport and electrochemical reaction. The GDL deformation model couples permeability and porosity with the thickness of the porous GDL, which enables the model's capability to simulate how the GDL deformation influences the fluid transport phenomena in the PEM fuel cell.

2. Numerical simulation

2.1. Modeling domain and modeling assumptions

The computational domain shown in Fig. 2 includes the cathode GDL and serpentine flow channels of a 1 cm^2 fuel cell. The catalyst layer was assumed to be infinitely thin. The along-the-channel direction, the in-plane direction, and the direction perpendicular to the membrane are denoted as x, y, and z, respectively. There are five channels on the bipolar plate, and each channel has a width of 1 mm, a height of 1 mm, and a length of 10 mm. The width of the channel shoulder is 1 mm.

The present model is developed under the following assumptions:

(1) The fuel cell operates at a constant temperature.
(2) The gas mixture behaves like ideal gases.
(3) The gas flow is assumed to be laminar and incompressible in the modeling domain.
(4) The GDL material is assumed to be isotropic and non-homogenous.

(5) Although the liquid water presence is important in the PEM fuel cell operation, the liquid transport is ignored in the current work because the focus of this work is to study the flow crossover effect under the shoulder of bipolar plates with the GDL deformation. Therefore, water is assumed to be vapor in the gas mixture, and single phase flow is considered.

Based on the aforementioned model domain and assumptions, two numerical models are developed. One is to describe the GDL's deformation due to the assembly compression, and the other is to predict the fuel cell performance. The deformation model was solved first to obtain the deformed GDL geometry. This deformed geometry was then re-meshed to provide the computational domain for the PEM fuel cell model. These two models will be introduced in the next two sections.

2.2. The GDL deformation model

The deformation of the GDL due to the assembly compression is solved as a structural mechanics problem and finite element analysis (FEA) will be applied. The computational domain is shown in Fig. 2. In the model, the x and y coordinates are fixed and deformation occurs only in the z direction, which corresponds to the direction of the compression force.

In the structural mechanics model, the GDL-10BA from Mishra et al. [17] was used with the Poisson's ratio of 0.09, Zhang et al. [18]. The nominal clamping pressure applied is typically between 0.5 and 3 MPa [17]. In this model, 1 MPa of clamping pressure is applied. The mechanical properties of the GDL-10BA are shown in Table 1.

To protect the membrane and GDL and to prevent leakage, a layer of incompressible gasket frame is often added between the GDL
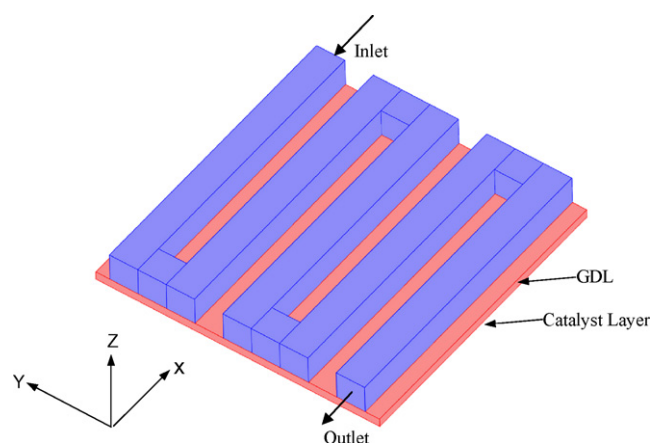

Fig. 2. Computational domain of a single serpentine PEM fuel cell model.

Table 1
Mechanical properties of GDL-10BA in FEA analysis

Parameter name	Value	Unit	Source
Compression modulus of the GDL	4.59	MPa	[17]
Poisson ratio	0.09	1	[18]
Compression pressure	1	MPa	Estimated
GDL max compression	0.075	mm	[19]

and bipolar plate during the fuel cell assembly, which adds a constraint for the GDL deformation. In the current structural mechanics model, the maximum deformation of GDL is set as 75 μm [19].

Fig. 3 shows the cross-sectional view of the GDL meshes with and without the assembly compression being considered. Due to the assembly compression, the thickness of the GDL is decreased under the shoulder of bipolar plates while a portion of the GDL extrudes into the gas channel. For the GDL-10BA gas diffusion layer with a thickness of 300 μm employed in the work, the GDL displacement could be more than 75 μm under the 1 MPa compression if there is no protection from the incompressible gasket layer. With the protection of the incompressible gasket, the compression ratio of the GDL in the present study is 75/300 = 0.25.

The porosity and permeability of GDL are two key parameters affecting the reactant transport inside the fuel cell. The values of these two parameters vary as the thickness of the GDL changes. Therefore, the porosity and permeability of GDL are not homogenous, and they need to be recalculated when the assembly compression is considered. In the present study, the porosity of the GDL is assumed to vary with the GDL thickness by the following relation [20]:

$$\varepsilon = 1 - W_A/(\rho D) \tag{1}$$

where W_A is the area weight of porous materials, $\mathrm{kg\,m^{-2}}$; ρ is the solid phase density, $\mathrm{kg\,m^{-3}}$; D is the thickness of the GDL, m. The variation of GDL permeability with the change of the GDL porosity is described by the following relation as suggested by Berning [21]:

$$K = \frac{K_0}{\varepsilon_0}\left(\frac{d}{d_0}\right)^2\left(1 - (1-\varepsilon)\frac{d_0}{d}\right) \tag{2}$$

where d is the pore diameter of porous media, m, which is assumed to be proportional to the thickness of GDL, ε is the porosity, and the subscript "0" denotes the original value of the parameter without

Fig. 3. Deformed computational domain of the PEM fuel cell model (*top*: without compression; *bottom*: with compression).

compression. The values of newly calculated porosity and permeability will be used in the PEM fuel cell model introduced in the next section.

2.3. PEM fuel cell model

2.3.1. Governing equations

The governing equations of fuel cell models are summarized and presented in each computational domain as shown below:

Flow channels: the steady-state Navier–Stokes equation and the continuity equation are solved to obtain the gas flow field and pressure field, i.e. the continuity equation:

$$\nabla \cdot u = 0 \tag{3}$$

and the momentum equation:

$$\rho u \cdot \nabla u = \nabla \cdot [-pI + \eta(\nabla u + (\nabla u)^{\mathrm{T}})] \tag{4}$$

where u is the velocity vector, $\mathrm{m\,s^{-1}}$; ρ is the fluid density, $\mathrm{kg\,m^{-3}}$; p is the pressure, Pa; η is the dynamic viscosity, $\mathrm{kg\,m^{-1}\,s^{-1}}$.

Flow in the GDL: in the gas diffusion layer, the pressure drop is proportional to the gas velocity if the flow is laminar, and it is modeled as

$$(\eta/\kappa)u = \nabla \cdot [-pI + (1/\varepsilon)\eta(\nabla u + (\nabla u)^{\mathrm{T}})] \tag{5}$$

where k is the permeability of the GDL, $\mathrm{m^2}$, and ε is the porosity.

The multi-species mass transport in the entire computational domain (including the gas channels and GDL) are described by the Maxwell–Stefan equation. It solves for the fluxes of each species in terms of mass fraction. The general form of the Maxwell–Stefan equation is shown below:

$$\nabla \cdot \left[-\rho w_i \sum_{j=1}^{N} D_{ij}\left\{\frac{M}{M_j}\left(\nabla w_j + w_j\frac{\nabla M}{M}\right) + (x_j - w_j)\frac{\nabla P}{P}\right\} + w_i\rho u\right]$$
$$= R_i \tag{6}$$

where D_{ij} is the binary diffusion coefficient; R_i is the reaction rate; x is the molar fraction; w is the mass fraction; M is the molecular mass; i and j represent different species O_2, H_2O or N_2 and ρ is the mixture gas density described by

$$\rho = \frac{\left(\sum_i x_i M_i\right) p}{RT} \tag{7}$$

where R is the universal gas constant, $8.314\,\mathrm{J\,mol^{-1}\,K^{-1}}$ and T is the cell operating temperature. On the cathode side, the mass fractions of oxygen and water are solved since the mass fraction of nitrogen can always be obtained from the mass balance equation as follows:

$$w_{N_2} = 1 - w_{O_2} - w_{H_2O} \tag{8}$$

The catalyst layer is treated as an infinitely thin boundary between the GDL and membrane. The Tafel equation is used to predict the distribution of the current density along the catalyst layer [22]:

$$I = I_0\frac{C^g y_{O_2}}{C_{O_2,\mathrm{ref}}}\exp\left(\frac{\alpha_c F}{RT}\eta_c\right) \tag{9}$$

where I_0 is the exchange current density, $\mathrm{A\,cm^{-2}}$; η_c is the overpotential on the cathode side, V; α_c is the cathode transfer coefficient; F is the Faraday's constant; C is the concentration of gas, $\mathrm{mol\,m^{-3}}$.
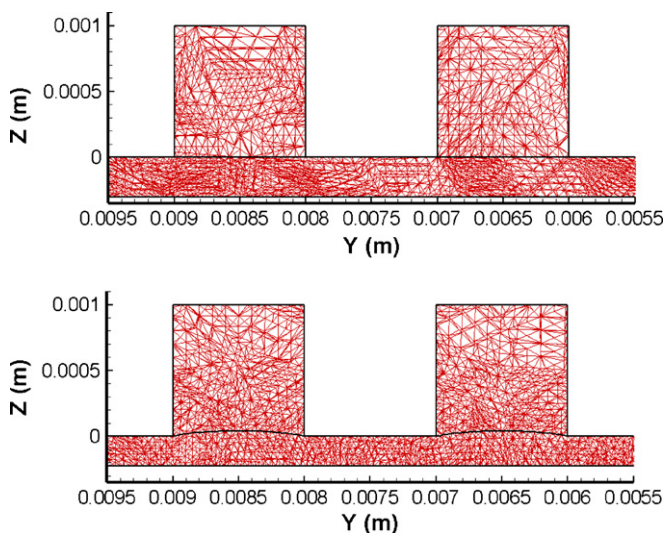
2.3.2. Boundary conditions

(1) *Flow inlet*: The inlet gas velocity and species fraction are calculated based on the mass flow rate and humidified air components, respectively.
(2) *Flow outlet*: At the outlet, the back pressure is set to the atmospheric pressure. The flow is assumed to be fully developed.
(3) *Impermeable walls and surfaces*: A no-slip boundary condition is applied to the impermeable walls and surfaces, where the no-flux condition is set for the species equations.
(4) *Catalyst layer*: At the membrane–GDL interface, the catalyst layer is assumed to be an infinitely thin layer, where the boundary condition of the momentum equation is set to no slip and the fluxes of oxygen and water are the functions of the local current density, and they are given as

$$\text{oxygen}: \quad N_{O_2} = -\frac{I}{4F} \tag{10}$$

$$\text{water}: \quad N_{H_2O} = (0.5 + \alpha)\frac{I}{F} \tag{11}$$

where N is the inward mass flux and α is the number of water molecules dragged across the PEMFC membrane for each electron transferred.

3. Result and discussion

The aforementioned structural mechanics model and the PEM fuel cell model were implemented into the commercial software package COMSOL Multiphysics. The base case parameters used in both models are listed in Table 2. The anode overpotential is ignored due to the much faster reaction compared to that on the cathode side. The fuel cell operating potential is therefore calculated as

$$V_{cell} = V_{oc} - \eta_c - IR_{cell} \tag{12}$$

where V_{cell} is the fuel cell operating voltage; V_{oc} is the open circuit voltage; η_c is the cathode overpotential; I is the fuel cell operating current density; R_{cell} is the ohmic electrical resistance of the fuel cell.

Table 2
Base model parameters

| Parameter name	Value	Unit	Source
Geometry dimensions			
Channel depth	1	mm	
Channel width	1	mm	
Should width	1	mm	
GDL thickness	0.3	mm	
Active area	1	cm^2	
Base case operating conditions			
Inlet gas velocity	3	m s^{-1}	Estimated
Inlet mole fraction of oxygen	0.150	1	Humidified air at 80 °C
Inlet mole fraction of nitrogen	0.495	1	Humidified air at 80 °C
Inlet mole fraction of water	0.355	1	Humidified air at 80 °C
Temperature	80	°C	Typical
Back pressure	101,325	Pa	
Other properties and coefficients			
Gas dynamic viscosity	2.03E−5	Pa s	[22]
Exchange current density	1E−2	A cm^{-2}	[22]
Transfer coefficient of the oxygen reduction reaction	0.5	1	[22]
Electrode permeability	1.76E−11	m^2	[22]
Electrode porosity	0.5	1	Estimated
Binary diffusion coefficient $D_{O_2\_N_2}$	2.75E−5	m^2 s^{-1}	[23]
Binary diffusion coefficient $D_{O_2\_H_2O}$	3.50E−5	m^2 s^{-1}	[23]
Binary diffusion coefficient $D_{H_2O\_N_2}$	3.50E−5	m^2 s^{-1}	[23]
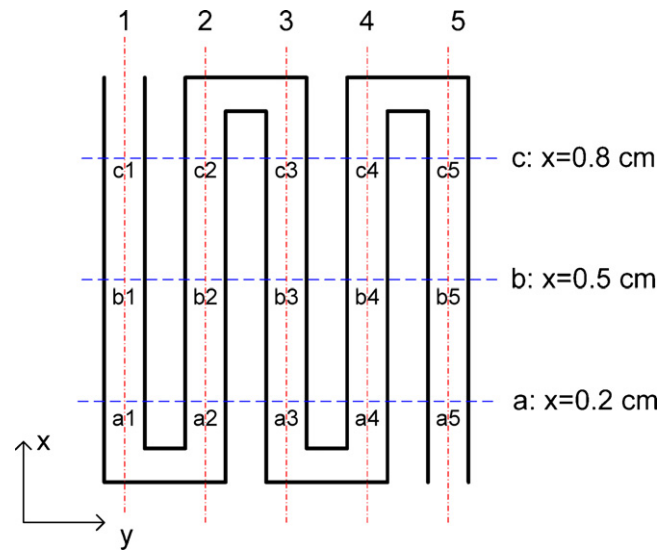
Fig. 4. 2D segmented modeling geometry.

In order to clearly explain the flow crossover effect, the original modeling geometry is segmented in several regions as shown in Fig. 4. The three horizontal lines are denoted by a, b and c, respectively. The five vertical lines are numbered numerically according to each channel. The horizontal line and vertical line designations are used to indicate the intersection point of two lines such as c1, b2, a5 and so on.

3.1. Pressure distribution and velocity field

Fig. 5 shows the comparison of the pressure drop along the flow direction at the cross section of $x = 0.8$ cm with and without assembly compression considered. The local pressure drop is normalized by the maximum pressure drop from inlet to the outlet. Pressure decreases from the inlet to outlet of the flow channel. A higher total pressure drop is found when the compression effect is considered. This pressure drop is due to the extra flow resistance caused by the deformation of the porous GDL material. Fig. 6 shows the comparison of the pressure drop between the adjacent flow channels for three different cross section locations a, b and c as indicated in Fig. 4. The pressure difference between c1 and c2 is approximately 155% higher than the one between c2 and c3. The reason is that there is a longer flow path from c1 to c2 than from c2 to c3. The pressure drop
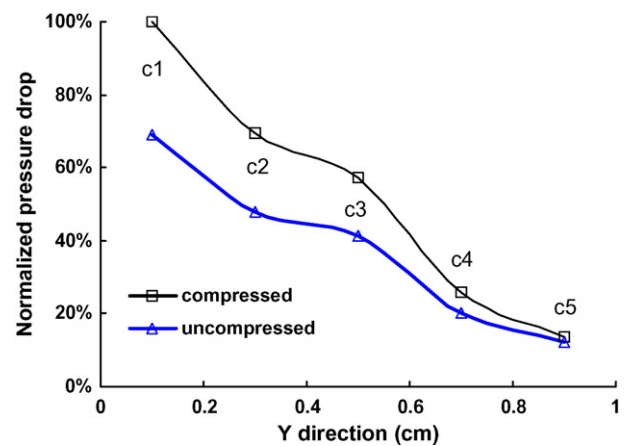

Fig. 5. Normalized pressure drop along the flow direction with and without assembly compression (c: $x = 0.8$ cm).
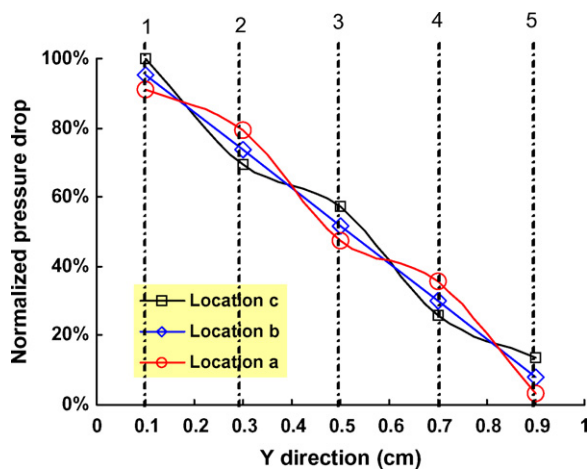
Fig. 6. Normalized pressure drop between the adjacent channels under compression at: (a) $x = 0.2$ cm, (b) $x = 0.5$ cm and (c) $x = 0.8$ cm.

between other points follows a similar trend. For example, the pressure drop between a1 and a2 is lower than the one between a2 and a3. The pressure difference between adjacent channels influences the flow crossover and also affects fuel cell performance.

Fig. 7 shows the gas velocity vector in the cross sectional plane with and without considering the assembly compression. Only the first two channels in Fig. 4 are presented here. Due to a high pressure difference between c1 and c2, more flow crosses the GDL from channel 1 to channel 2. At the location a, the flow crossover from a1 to a2 is much smaller compared to that from c1 to c2. When the assembly compression is considered, the flow crossover between adjacent channels decreases in spite of the fact that the pressure drop increases due to the compression. The reason is that the porosity and permeability of the GDL decreases after the GDL is compressed.

In the PEM fuel cell modeling, the reactant was often assumed to reach the catalyst layer only by diffusion transport [24]. The convective transport between adjacent channels in the GDL as shown in Fig. 7, however, should not be ignored.

3.2. Oxygen mass fraction and local current density

A direct result of the enhanced convective transport due to the higher pressure gradient between the adjacent channels is the shift of the reactant concentration. This concentration shift is very obvious in the GDL under the shoulder of bipolar plates. Fig. 8 shows the oxygen mass fraction with and without the assembly compression considered. The oxygen mass fraction decreases along the channel as oxygen is consumed along the channel. In the GDL, there is a more obvious oxygen concentration shift from c1 to c2 than from a1 to a2, which is consistent with the high flow crossover found in Fig. 7. A higher oxygen concentration is found for the case without considering the GDL deformation caused by assembly compression, which leads to an over-predicted fuel cell performance as shown later.

Fig. 9 compares the local current density distribution at the cathode catalyst layer with and without the assembly compression considered. Fig. 10 compares the local current density along the y direction at $x = 0.2$, 0.5 and 0.8 cm. The current density decreases along the flow direction. The local current density is high under the flow channel and low under the shoulder of the bipolar plate. The gas crossover between the adjacent channels changes the local current density distribution pattern especially under the bipolar plate shoulder. As shown in Fig. 10, due to the flow crossover, the
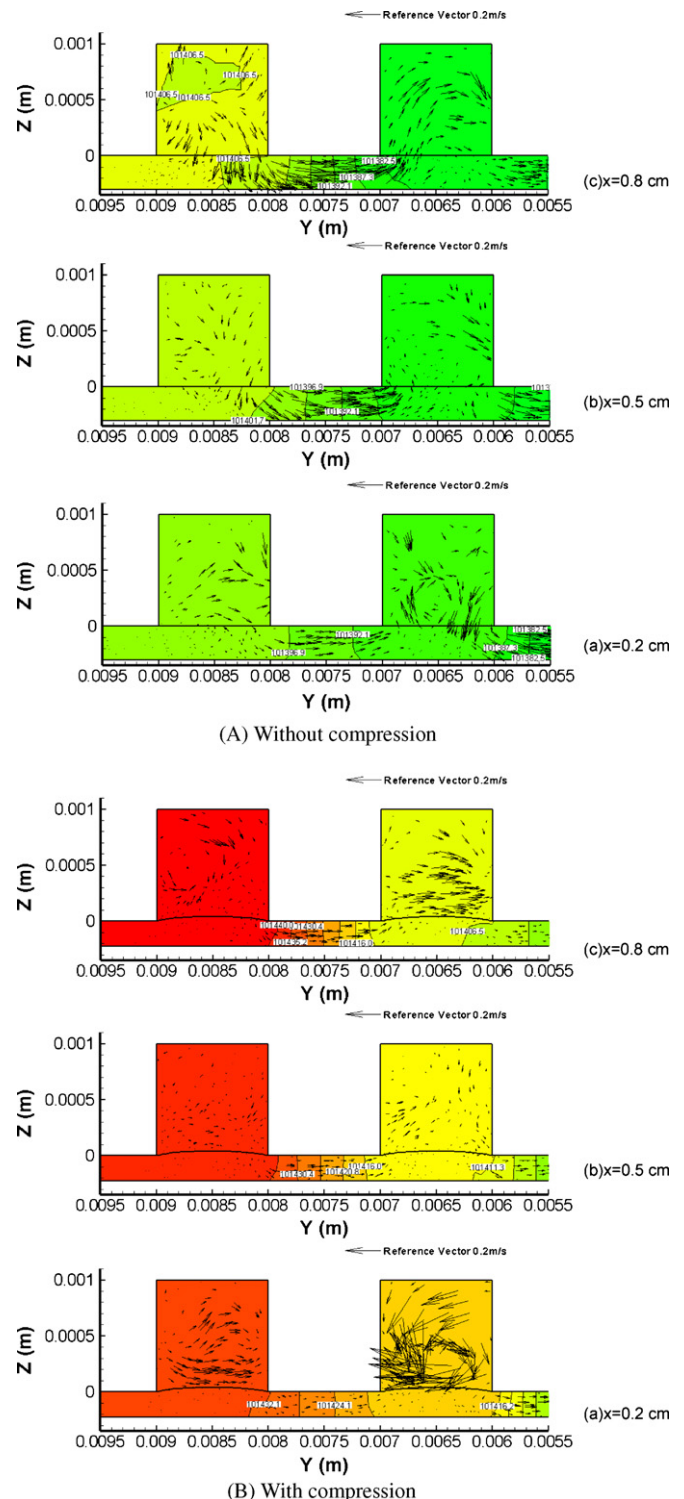

Fig. 7. Pressure distribution and gas velocity through the GDL. (A) Without compression; (B) with compression.

maximum and minimum values of the local current density at each channel shift from the center of either channel or land to the flow crossover direction. The shift of the current density is more obvious for the region with more flow crossover such as from c1 to c2, c3 to c4 and so on. Additionally, the flow crossover enhances the overall uniformity of the local current density distribution. The reduced flow crossover due to compression shown in Fig. 7B decreases the
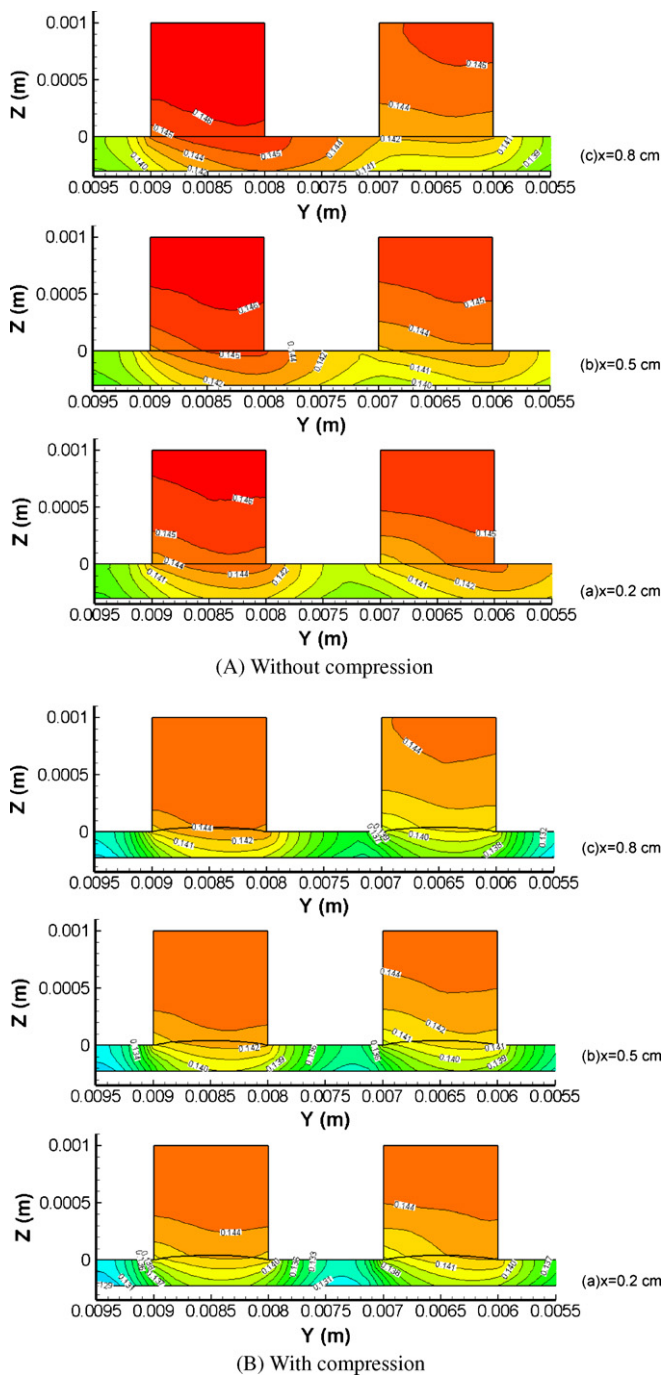
Fig. 8. Oxygen mass fraction distributions on the cathode channel and GDL. (A) Without compression; (B) with compression.

uniform distribution of the local current density shown in Fig. 9B. Comparing Fig. 9A and B, it is concluded that without assembly compression considered, the over-predicted mass transport of oxygen, as shown in Fig. 8A, results in a over-predicted local current density at the cathode catalyst layer. This again explains the necessity of adding the compression analysis into the modeling of the fuel cell with a serpentine channel.

3.3. Quantity of the flow crossover

To quantitatively describe the flow crossover between adjacent channels, the oxygen crossover ratio is defined as the percentage
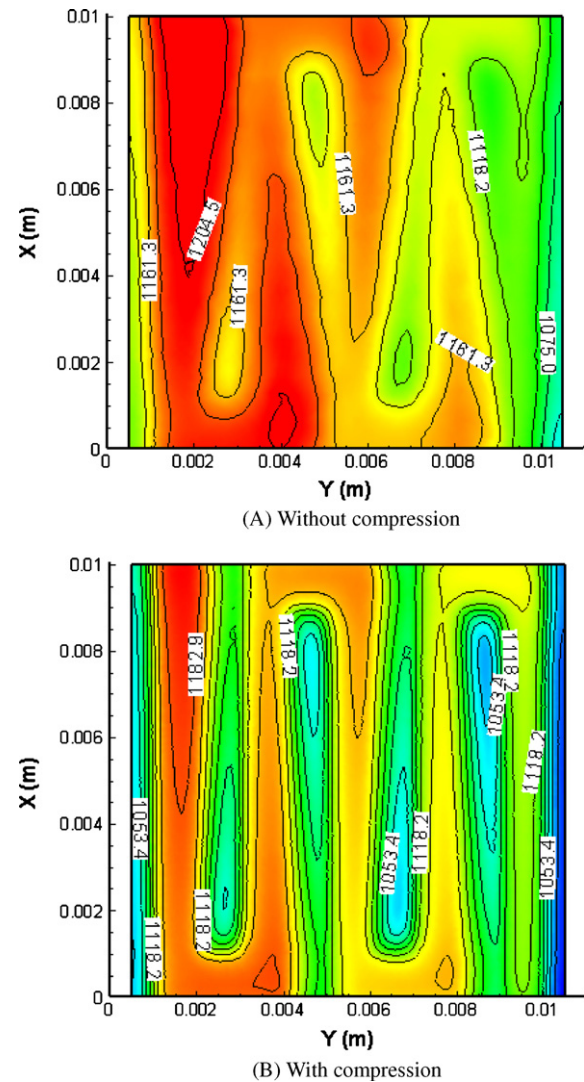

Fig. 9. Local current density at the cathode catalyst layer ($A\,m^{-2}$). (A) Without compression; (B) with compression.
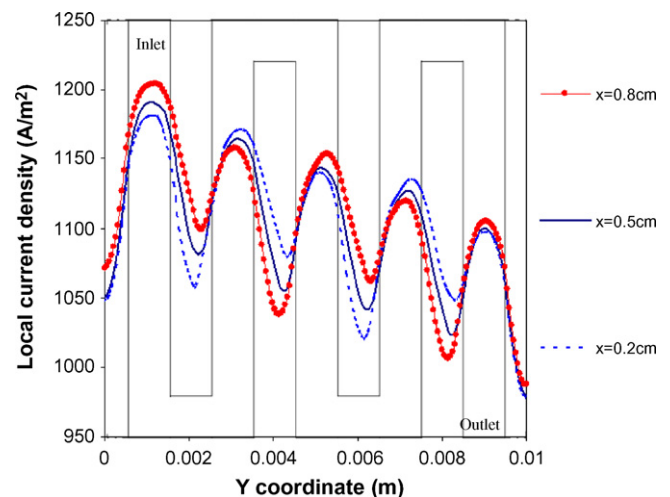

Fig. 10. Local current density at cross section ($x = 0.2$, 0.5 and 0.8 cm).
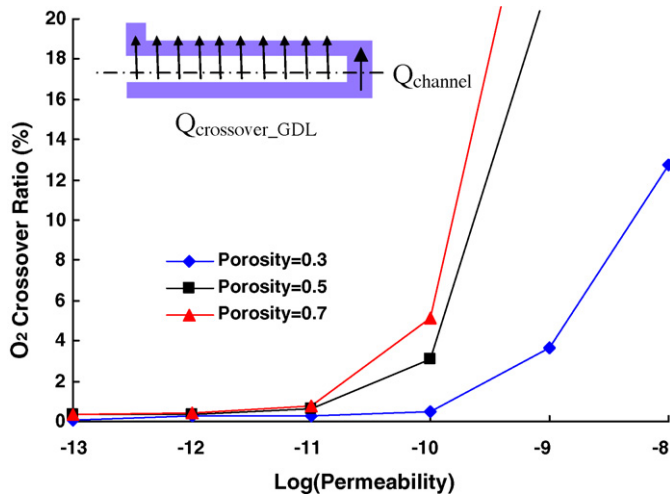
Fig. 11. Ratio of the oxygen flux through GDL over the total oxygen flux.

of the oxygen mass flux through the first land area between the first and second flow channel from the inlet (represented by $Q_{crossover\_GDL}$) to the total oxygen mass flux from the first channel to the second (represented by $Q_{crossover\_GDL} + Q_{channel}$). So the ratio is then

$$\gamma = \frac{\dot{Q}_{cross\_GDL}}{\dot{Q}_{cross\_GDL} + \dot{Q}_{channel}} \qquad (13)$$

The permeability and porosity of the GDL describe the porous GDL's capability to transport the reactant gas to the active catalyst layer. The flow crossover between adjacent channels is significantly affected by both parameters. Fig. 11 shows the oxygen crossover ratio in channel 1 of Fig. 4 as a function of the permeability and porosity. The crossover increases with the increase of either porosity or permeability. This indicates that a GDL which is highly porous and permeable enhances oxygen transport between the channels, and contributes to a more even distribution of the water and heat generation. Considering that typical values of the permeability and porosity of GDL are 10^{-11} m^2 and 0.5, the crossover ratio could be about 1–2% at the first land for this particular case. If the fuel cell size increases from 1 to 100 cm^2 and the flow crossover at all the lands are added, the total amount of crossover could significantly increase and therefore influence the total fuel cell performance.
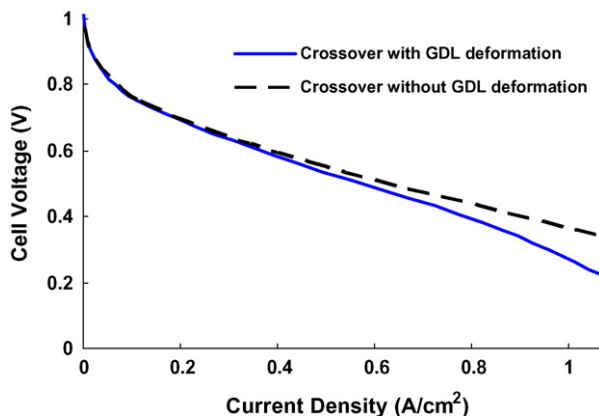

Fig. 12. Polarization of the serpentine channel fuel cell modeling.

3.4. Polarization curve

Fig. 12 shows the polarization curve comparison with and without considering the assembly compression. The gas crossover through the GDL is driven by the pressure difference between two adjacent channels. The permeability is the property which directly affects the flow crossover. It decreases when the fuel cell is compressed, and thus the compression influences the fuel cell performance in an indirect way. The performance of the PEM fuel cell decreases due to the assembly compression, especially at the high current density region. This is consistent with the previous analysis where the flow crossover decreases due to the assembly compression shown in Fig. 7B as well as the oxygen concentration shown in Fig. 8B. This effect would be more obvious if a longer serpentine channel fuel cell is used.

4. Conclusions

For a PEM fuel cell with the serpentine flow channel design on the bipolar plate, the flow crossover between adjacent flow channels affects the local current density distribution, and thus influences the fuel cell performance. The flow crossover across the GDL changes due to the assembly compression from the shoulder of bipolar plates.

A structural mechanics model was developed to study the deformation of the GDL under the assembly compression. A deformed geometry was created from the FEA analysis. The permeability and porosity of the deformed GDL was recalculated. A three-dimensional PEM fuel cell model was developed based on the deformed geometry and the recalculated porosity and permeability of a GDL, which improved the accuracy of the fuel cell model. This model was used in the present study to investigate the flow crossover effects. The following conclusions are drawn from the current study:

(1) The flow crossover is driven by the pressure difference between two adjacent channels, and the permeability of GDL also affects the amount of flow crossover.
(2) As a result of flow crossover between adjacent channels, there exists an oxygen concentration shift from the channel center to the adjacent channel, and it is more obvious without considering the assembly compression. The local current density distribution at the catalyst layer also shows a similar shift from the channel center to the adjacent channel.
(3) To quantitatively describe the flow crossover between adjacent channels through the GDL, the oxygen crossover ratio was defined, and a parametric study was conducted to investigate the permeability and porosity of the GDL's effect on this ratio. It was found in the fuel cell that at the typical values of GDL permeability and porosity (10^{-11} m^2 and 0.5), the cross over ratio is about 1–2% at the first channel for the fuel cell investigated in this study. The total amount of flow crossover will increase if the fuel cell size increases.
(4) The pressure drop from the inlet to the outlet of the flow channel increases due to the assembly compression.
(5) The flow crossover from one channel to the adjacent channel decreases when the assembly compression is considered, as well as the performance of fuel cell especially in the high current density region.

In summary, the present study shows that the crossover effect is important in the fuel cell with serpentine channels and the effect of the assembly compression is crucial in the high current density region, and should be incorporated into the PEM fuel cell simulation

and design. Without considering the GDL deformation, the fuel cell model overpredicts the fuel cell performance.

References

[1] X. Li, Principles of Fuel Cells, Taylor & Francis, 2006.
[2] J. Park, X. Li, J. Power Sources 163 (2007) 853–863.
[3] P.H. Oosthuizen, L. Sun, K.B. McAuley, Appl. Therm. Eng. 25 (2005) 1083–1096.
[4] S. Dutta, S. Shimpalee, J.W. Van Zee, Int. J. Heat Mass Transfer 44 (2001) 2029–2042.
[5] L. Sun, P.H. Oosthuizen, K.B. McAuley, Proceedings of the Hydrogen and Fuel Cells 2004 Conference and Trade Show, September 25–28, Toronto, Ontario, Canada, 2004.
[6] L. Sun, P.H. Oosthuizen, K.B. McAuley, Int. J. Therm. Sci. 45 (2006) 1021–1026.
[7] Q. Ye, T.S. Zhang, C. Xu, Electrochim. Acta 51 (2006) 5420–5429.
[8] J. Pharoah, J. Power Sources 144 (1) (2005) 77–82.
[9] W. Chang, J. Hwang, F. Weng, S. Chan, J. Power Sources 166 (2007) 149–154.
[10] W. Lee, A.C. Ho, J.W. Van Zee, M. Murthy, J. Power Sources 84 (1999) 45–51.
[11] P. Zhou, C. Wu, G. Ma, J. Power Sources 159 (2006) 1115–1122.
[12] J. Ge, A. Higier, H. Liu, J. Power Sources 159 (2006) 922–927.
[13] P. Zhou, C. Wu, G. Ma, J. Power Sources 163 (2007) 874–881.
[14] Z. Shi, X. Wang, ECS Trans. 11 (1) (2007) 637–646.
[15] P. Zhou, C. Wu, J. Power Sources 170 (2007) 93–100.
[16] Y. Lai, P.A. Rapaport, C. Ji, V. Kumar, J. Power Sources 184 (1) (2008) 120–128.
[17] V. Mishra, F. Fang, R. Pitchumani, J. Fuel Cell Sci. Technol. 1 (2004) 2–9.
[18] L. Zhang, Y. Liu, H. Song, S. Wang, Y. Zhou, S.J. Hu, J. Power Sources 162 (2006) 1165–1171.
[19] 50 AMP AMREL Load Fuel Cell Test Station Manual, Fuel Cell Technologies Inc., 2007.
[20] F. Barbir, PEM Fuel Cells Theory and Practice, Elsevier Academic Press, 2005.
[21] T. Berning, Three-dimensional computational analysis of transport phenomena in a PEM fuel cell, Ph.D. Dissertation, University of Victoria, Canada, 2002.
[22] W. He, J.S. Yi, T.V. Nguyen, AIChE J. 46 (10) (2000) 2053–2064.
[23] J.A. Wesselingh, R. Krishna, Mass Transfer in Multicomponent Mixtures, Delft University Press, 2000.
[24] G. Lin, T.V. Nguyen, J. Electrochem. Soc. 153 (2) (2006) A372–A382.